ISSN 2176-5480

22nd International Congress of Mechanical Engineering (COBEM 2013)
November 3-7, 2013, Ribeirão Preto, SP, Brazil

VALIDATION OF LES SIMULATION OF A TURBULENT RADIANT FLAME USING OPENFOAM

Yuri Paixão de Almeida
Escola de Química - EQ/UFRJ
ypaixaoalmeida@gmail.com

Paulo Laranjeira da Cunha Lage
Programa de Engenharia Química - PEQ/COPPE/UFRJ
paulo@peq.coppe.ufrj.br

Luiz Fernando Lopes Rodrigues Silva
Escola de Química - EQ/UFRJ
lflopes@eq.ufrj.br

Abstract. *Combustion phenomena occurs in many engineering applications as equipment design and fire safety. In this context, Computational Fluid Dynamics (CFD) applied to the numerical simulation of flames is a growing field that improves the understanding of combustion. Experimental data from the literature for an established methane flame on a diffuser burner with exit diameter of 7.1 cm, fuel flow rate of 84.3 mg/s and burning in an open environment were used for the CFD model validation. Simulations were performed in FireFOAM, a compressible flow solver for flame simulation implemented in the open-source CFD package OpenFOAM. The eddy dissipation combustion model (EDM) with single-step reaction between methane and air was employed. Soot production was neglected. Conservation of chemical species was modeled by the individual species transport equations. Thermal radiation was solved by Finite Volume Discrete Ordinate Method (FVDOM) using the Planck mean absorption coefficient. Large Eddy Simulation (LES) was used for the turbulence modeling, using the one equation eddy model to solve for the eddy viscosity. The grid-size independence of the simulations was verified. Finally, the simulated profiles for velocities and mixture fractions were compared to their measurements available in the literature with good agreement.*

Keywords: *CFD, flame, combustion, radiation, OpenFOAM*

1. INTRODUCTION

Despite the continuous search for renewable fuels, oil holds a leading position as raw material for power generation, especially with the increasing of its reserves due to new technologies for exploration. Power generation from petroleum derivatives occurs through the burning of these fuels in boilers, turbines and internal combustion engines. In the context of project equipment, adequate understanding of the phenomena involving thermal exchanges with thermal radiation is of crucial interest to reduce costs through lower fuel consumption. Furthermore, oil is a high flammable fluid and has associated risk in all its stages of production. The safety engineering seeks to reduce these risks and the correct combustion modeling becomes essential for fire hazard analysis, active and passive fire protection design and equipment dimensioning accidental load (DAL) calculation.

Therefore, appropriate analysis of combustion phenomena represents a key role in many areas of engineering and, due to the complexity of its modeling, usually the development of mathematical correlations from experimental data is applied to it. However, in specific cases in which there is no validation for these correlations, this approach has reduced reliability and conducting experiments may presents high cost to collect reliable data.

Alternatively to such models, the computational fluid dynamics (CFD) emerges as a possible option for the numerical modeling, since the resolved conservation equations have strong physical basis and not only agreement with experimental measurements. The CFD combustion modeling from the conservations equations of mass, *momentum* and energy has grown in importance due to a dramatically increase in computational capacity, previously a limiting factor. However, reviews of the techniques and main challenges has been shown (Veynante and Vervisch, 2002; McGrattan, 2005) that consistent results are still rare.

This paper presents the use of OpenFOAM, an open-source CFD package, for flame modeling. Another open-source software used to perform combustion simulations is the Fire Dynamics Simulator - FDS (Sandia), considered by the most of the available literature, such as Xin *et al.* (2005, 2008); Skarsbø (2011); Wen *et al.* (2006). Nevertheless, FDS employs a limited number of mathematical methods for turbulence, thermal radiation and reactions. Furthermore, it also has strong limitations in the treatment of complex geometries because it only supports full orthogonal meshes.

Alternatively, OpenFOAM handles non-orthogonality very well, presenting an excellent environment for code development due to its object-oriented language C++. Besides, it is easily scalable in parallel processing and provides a wide

ISSN 2176-5480

range of options of discretization methods and linear system solvers. The FireFOAM, a code developed by FM Global using OpenFOAM, combines the necessary characteristics for flame simulation. It is important to mention that combustion simulations presents a highly difficult level due to the strong coupling between chemistry, turbulence and thermal radiation, requiring a detailed model to simulate them. In this work, the methods and the physical modeling employed by FireFOAM are presented. The results for a validation case of a methane flame on a diffuser burner, documented in the literature (Zhou and Gore, 1998; Xin *et al.*, 2005), are also presented.

2. METHODOLOGY

In the following, the models that are implemented in FireFOAM are described as well as the hypotheses and simplifications that were used to solve the validation case.

2.1 Governing equations

The classic hypothesis of continuum mechanics is used and the continuity equation, considering Favre filtering for LES turbulence modeling, takes the form:

$$\frac{\partial \overline{\rho}}{\partial t} + \nabla \cdot (\overline{\rho}\widetilde{\mathbf{u}}) = 0 \tag{1}$$

where $\overline{\rho}$ and $\widetilde{\mathbf{u}}$ are the density and velocity, respectively. In this work, whenever a variable presents a "-"above its symbol it is a filtered variable and when it presents a "~", it is a filtered density-weighted variable. In order to consider the gas compressibility, the ideal gas law was employed:

$$\overline{\rho} = \left(\sum_{i=1}^{N} \frac{M_i}{\widetilde{Y}_i R} \right) \frac{\overline{p}}{\widetilde{T}} \tag{2}$$

where i is an index representing each chemical specie, M_i and $\widetilde{Y}_i$ represents the molar mass and mass fraction of each specie, N is the number of chemical species, R is the ideal gas constant, $\overline{p}$ means the thermodynamic pressure and $\widetilde{T}$ is the temperature.

The *momentum* conservation equation, considering a Newtonian fluid, takes the form:

$$\frac{\partial \overline{\rho}\widetilde{\mathbf{u}}}{\partial t} + \nabla \cdot (\overline{\rho}\widetilde{\mathbf{u}}\widetilde{\mathbf{u}}) = -\nabla \overline{p_d} - (\mathbf{g} \cdot \mathbf{x}) \nabla \overline{\rho} + \nabla \cdot \left[\mu_{eff} \left(\nabla \widetilde{\mathbf{u}} + (\nabla \widetilde{\mathbf{u}})^T - \frac{2}{3} (\nabla \cdot \widetilde{\mathbf{u}}) \mathbf{I} \right) \right] \tag{3}$$

where $\mathbf{I}$ represents the identity tensor, μ_{eff} is the effective viscosity and $\mathbf{g}$ and $\mathbf{x}$ are the gravity and the position vectors. It should be noted that the pressure to be solved is not the thermodynamic pressure $\overline{p}$, but the dynamic pressure $\overline{p_d}$, defined as:

$$\overline{p_d} = \overline{p} - \overline{\rho}\mathbf{g} \cdot \mathbf{x} \tag{4}$$

As cited by Ferziger and Peric (2004), it is convenient to solve for the dynamic pressure instead of the thermodynamic pressure to improve numerical solution effectiveness. The isotropic part of the sub-grid scale stress tensor, $(2/3)\rho k$, where k is the turbulent kinetic energy, is usually incorporated by the definition of a modified pressure. However, this term can be neglected for Mach < 0.4 (Erlebacher *et al.*, 1991) and, therefore, it was not considered in the present work. The effective viscosity, μ_{eff}, is the sum of the dynamic viscosity, μ, and the sub-grid scale eddy viscosity, μ_{sgs}. The Sutherland's viscosity law was used to calculate μ.

The reaction model considers an infinitely fast single-step reaction, neglecting soot production, which is a good approximation for a small methane flame:

$$CH_4 + 2O_2 + 7.52N_2 \longrightarrow CO_2 + 2H_2O + 7.52N_2 \tag{5}$$

Four individual species transport equations are solved to determine the gas composition:

$$\frac{\partial \overline{\rho}\widetilde{Y_i}}{\partial t} + \nabla \cdot \left(\overline{\rho}\widetilde{\mathbf{u}}\widetilde{Y_i} \right) = \nabla \cdot \left(\overline{\rho} D_{eff} \nabla \widetilde{Y_i} \right) + \overline{\omega_i}, \quad i = CH_4, O_2, H_2O, CO_2 \tag{6}$$

where the effective mass diffusivity, D_{eff}, is the sum of the diffusion coefficient for each species in the mixture, D_i, and the sub-grid scale mass diffusivity, D_{sgs} and $\overline{\omega_i}$ represents the rate of consumption or production of species "i". N_2 is not calculated by a transport equation, being obtained by the closure relation:

$$\sum_{i=1}^{5} Y_i = 1 \tag{7}$$

ISSN 2176-5480

In this work, the rate of reaction of methane, $\overline{\omega_{CH_4}}$, is given by the eddy dissipation model (Yeoh and Yuen, 2009):

$$\overline{\omega_{CH_4}} = C_r \overline{\rho} \frac{\epsilon}{k} \, min \left[\widetilde{Y_{CH_4}}, \frac{\widetilde{Y_{O_2}}}{s} \right] \tag{8}$$

where C_r is a model constant being equal to 4 (Lupant *et al.*, 2007), ϵ is the eddy energy specific dissipation rate, k is the turbulent kinetic energy, Y_{CH_4} and Y_{O_2} are the methane and oxygen mass fraction, and s is the mass stoichiometric fraction. For the others species, $\overline{\omega_i}$ is easily obtained through stoichiometric relations.

The energy conservation equation is solved in terms of sensible enthalpy, $\widetilde{h_s}$:

$$\frac{\partial \overline{\rho} \widetilde{h_s}}{\partial t} + \nabla \cdot \left(\overline{\rho} \widetilde{\mathbf{u}} \widetilde{h_s} \right) = \frac{D\overline{p}}{Dt} + \nabla \cdot \left(\overline{\rho} \alpha_{eff} \nabla \widetilde{h_s} \right) + \overline{q_c} - \nabla \cdot \overline{\mathbf{q}_R} \tag{9}$$

where the effective thermal diffusivity, α_{eff}, is the sum of the mixture thermal diffusivity, α, and the sub-grid scale thermal diffusivity, α_{sgs}, $\overline{q_c}$ is the heat generated by combustion and $\overline{\mathbf{q}_R}$ is the thermal radiation flux that plays a major role in flame heat loss and shall be accurately modeled to ensure reliable results. The quantity $\overline{q_c}$ was obtained by:

$$\overline{q_c} = \Delta H_c^{\circ} \, \overline{\omega_{fu}} \tag{10}$$

where ΔH_c° is the heat of combustion of methane, whose value is -802.310 kJ/mol (Rogers and Mayhew, 1995). The thermal diffusivity, α, is calculated by:

$$\alpha = \frac{\gamma}{\overline{\rho} C_P} \tag{11}$$

where γ is the thermal conductivity, determined using the modified Eucken method (Poling *et al.*, 2001) and C_P is the heat capacity, calculated by the NIST-JANAF thermodynamic tables. For a methane flame, the assumption of unity Lewis number can be used without loss of accuracy, as discussed by Aspden *et al.* (2011). Therefore, we assumed $D_{eff} = \alpha_{eff}$.

Since the experimental data for gas concentration are provided in mixture fraction, F_t, our results had to be presented using it for comparison. The mixture fraction, F_t, is given by:

$$F_t = \frac{s\widetilde{Y_{CH_4}} - \widetilde{Y_{O_2}} + \widetilde{Y_{O_2}^{\infty}}}{s\widetilde{Y_{CH_4}^{f}} + \widetilde{Y_{O_2}^{\infty}}} \tag{12}$$

where $\widetilde{Y_{CH_4}^{f}}$ is the methane mass fraction at the fuel inlet and $\widetilde{Y_{O_2}^{\infty}}$ is the oxygen mass fraction in air. Figure 1 presents the relations between the mixture fraction and the mass fractions of all species assuming an infinite reaction rate. It should be pointed out that the reaction model utilized in the present work, given by Eq.(8), is a finite reaction rate model based on turbulent mixing. Figure 1 is shown for a better comprehension of the variable mixture fraction relationship to local composition.

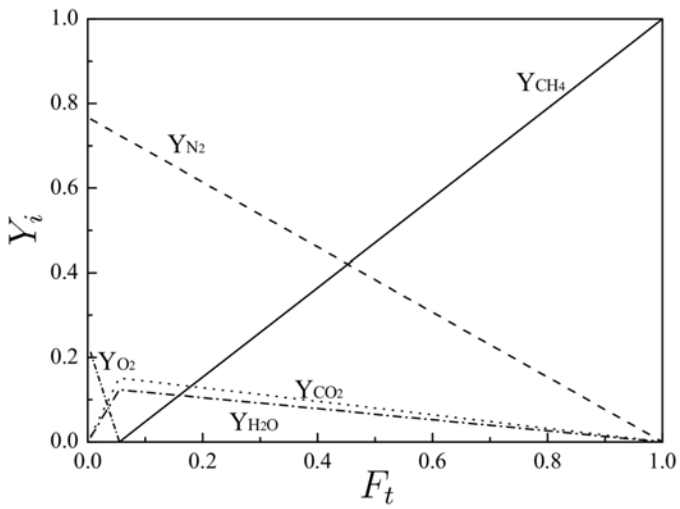

Figure 1. Mixture fraction composition relations for a methane reaction with air with infinite reaction rate - adapted from Zeng and Chow (2011).

ISSN 2176-5480

2.2 Radiation in participating media

Considering the five species present in the combustion system, only CH_4, H_2O and CO_2 participate in radiation, as O_2 and N_2 are diatomic molecules and do not present strong emission bands in the infrared region of the electromagnetic spectrum (Edge *et al.*, 2011). As soot is not appreciable produced in a small methane flame, scattering is neglected. Therefore, the spectral radiative transfer equation (RTE) is represented by:

$$\frac{dI_\lambda}{ds} = -\kappa_\lambda I_\lambda + \kappa_\lambda I_{b\lambda} \tag{13}$$

where λ represents the wavelength, I_λ is the spectral radiation intensity, $I_{b\lambda}$ is the spectral black body radiation intensity and κ_λ is the spectral absorption coefficient. The first and the second term on the right hand side of Eq. (13) represent the attenuation and augmentation of radiation by absorption and emission, respectively.

Using the definition of the Planck mean absorption coefficient and the assumption of an optically thin flame, Eq. (13) can be used to determine the divergence of the total radiation flux (Modest, 2003), which can be written as:

$$\nabla \cdot \mathbf{q}_R = \kappa \left(4\pi I_b - \int_{4\pi} I \, d\Omega \right) = \kappa_p \left(4\sigma T^4 - G \right) \tag{14}$$

where σ is the Stefan-Boltzmann constant, I is the total intensity, I_b is the total blackbody intensity, G is the total irradiance and κ_p is the mean Planck absorption coefficient. For each chemical specie, the Planck mean absorption coefficient, κ_p, is obtained by a function fitted to its dependence on temperature. Then, these are weighted according to the species concentration to obtain the mixture coefficient (Barlow *et al.*, 2001; Smith *et al.*, 2003).

The irradiance, G, have to be obtained by the numerical solution of the RTE. The Finite Volume Discrete Ordinates Method (FVDOM) has been constantly used to solve the irradiance in many CFD combustion problems and it was chosen for this work. It consists in splitting the radiation field in several discrete solid angles, calculating the radiation intensity for the mean directions within the chosen angles, and then using these values in an approximate integration on the overall solid angle to obtain the irradiance. The works of Siegel and Howell (1992), Modest (2003), Mishra and Roy (2007) and Mangani (2009) should be consulted for a full comprehension of FVDOM.

The radiation intensity for a control volume with volume V can be obtained after integration of Eq. (13) in volume and in the solid angle Ω in the form:

$$\sum_k I_k^m \left(\mathbf{D}^m \cdot \mathbf{n}_k \right) A_k = \kappa_{p,P} \left(I_{b,P}^m - I_P^m \right) V \Omega^m \tag{15}$$

where I_k^m is the radiation intensity in direction m over a face k, which has area A_k, $\mathbf{n}_k$ is the outward normal vector to A_k, and the index P indicates that the variables $\kappa_{p,P}$, $I_{b,P}$ and I_P are calculated ate the cell center. $\mathbf{D}^m$ is a vector pointing in an average direction within the solid angle element, Ω^m. It is defined as the integral in spherical coordinates of the direction vector, $\mathbf{s}$, in the solid angle interval, Ω^m:

$$\mathbf{D}^m = \int_{\Omega^m} \mathbf{s} \, d\Omega = \int_{\phi^m - \frac{\Delta\phi^m}{2}}^{\phi^m + \frac{\Delta\phi^m}{2}} \int_{\theta^m - \frac{\Delta\theta^m}{2}}^{\theta^m + \frac{\Delta\theta^m}{2}} \left(\sin\theta \sin\phi \, , \sin\theta \cos\phi \, , \cos\theta \right) \sin\theta \, d\theta d\phi \tag{16}$$

where θ is the polar angle and ϕ is the azimuthal angle. After calculating the I_P^m values for all control volumes and directions, it is possible to determine the irradiance by (Mishra and Roy, 2007):

$$G_P = \int_{4\pi} I_P \left(\theta, \phi \right) d\Omega \approx \sum_{k=1}^{M_\phi} \sum_{l=1}^{M_\theta} I_P^m \left(\theta_l^m, \phi_k^m \right) 2 \sin\theta_l^m \sin\left(\frac{\Delta\theta_l^m}{2} \right) \Delta\phi_k^m \tag{17}$$

where M_ϕ and M_θ are the number of azimuthal angles $(0 \leq \phi \leq 2\pi)$ and the polar angles $(0 \leq \theta \leq \pi)$ in the solid angle discretization, $\Delta\theta_l^m$ and $\Delta\phi_k^m$ represent the variations of the angles θ and ϕ, respectively, in the solid angle interval Ω^m. Knowing G, the discrete version of Eq. (14) gives the radiation flux divergence.

2.3 Turbulence Modeling

The Large Eddy Simulation (LES) model was employed because it is potentially more accurate than RANS models and capture the transient large-scale motion and intermittency of the buoyant fires (Xin *et al.*, 2005). Unity turbulent Prandtl number was assumed to calculate $\alpha_{sgs} = \nu_{sgs} = \mu_{sgs}/\rho$. The one equation eddy viscosity model is used to model the sub-grid scale stress tensor, $\boldsymbol{\tau}_{sgs}$:

$$\boldsymbol{\tau}_{sgs} = -2\mu_{sgs} \mathrm{dev}\left(\widetilde{\mathbf{S}} \right) + \frac{2}{3} \overline{\rho} k \mathbf{I} \tag{18}$$

ISSN 2176-5480

where dev($\widetilde{\mathbf{S}}$) is the deviatoric part of strain rate tensor $\widetilde{\mathbf{S}}$. The sub-grid scale viscosity, μ_{sgs}, is given by:

$$\mu_{sgs} = \rho C_k \Delta \sqrt{k} \tag{19}$$

where C_k is a constant equal to 0.094 (Xiao and Jenny, 2011) and Δ is the filter cutoff. The turbulent kinetic energy is obtained from the following conservation equation:

$$\frac{\partial \overline{\rho} k}{\partial t} + \nabla \cdot (\overline{\rho} \widetilde{\mathbf{u}} k) = \nabla \cdot (\mu_{eff} \nabla k) - \overline{\rho}\, \boldsymbol{\tau}_{sgs} : \widetilde{\mathbf{S}} - C_e\, \overline{\rho}\, \frac{k^{3/2}}{\Delta} \tag{20}$$

where C_e is a constant equal to 1.048 (Xiao and Jenny, 2011). In Eq. (20), $-\overline{\rho}\boldsymbol{\tau}_{sgs} : \widetilde{\mathbf{S}}$ represents the production rate of turbulent kinetic energy, while $-C_e\, \overline{\rho}\, \frac{k^{3/2}}{\Delta}$ is responsible for dissipation rate of this energy.

2.4 Numerical Procedure

The domain used for the simulations is cylindrical, with a height of 48.0 cm and a diameter of 42.6 cm. The methane inlet is a centralized circular disc with a diameter of 7.1 cm. A methane flow rate of 84.3 mg/s was imposed at this inlet with uniform gas velocity and without considering any perturbation that might break this symmetric configuration. The meshes used in the simulations are slightly non-orthogonal and corrections were applied to deal with this issue. The details of the meshes are presented in Tab. 1.

The second order backward differentiation scheme was employed for temporal discretization. The diffusive terms and the gradients were discretized using central differences. A total variation diminishing (TVD) scheme was used for the advective terms.

The discretized *momentum*, species transport and energy equations were solved by the preconditioned bi-conjugated gradient method (PBiCG). Generalized geometric-algebraic multi-grid method (GAMG) was employed to solve the discretized pressure equation originated from the application of momentum interpolation to the continuity equation. This method was also used to solve the discretized turbulent energy and the radiative transfer equations.

The convergence of the results regarding the number of discretized solid angle intervals used in the FVDOM was also carried out. First, the simulations were performed using 100 discretized solid angles obtained by using 20 subdivisions of the azimuthal angle interval, $(0 \leq \phi \leq 2\pi)$, and 5 subdivisions of the polar angle range, $(0 \leq \theta \leq \pi)$. Then, the convergence of the results was verified by other simulations using 320 discretized solid angles, which were obtained by using 32 subdivisions in the azimuthal angle interval and 10 subdivisions in the polar angle range.

The FireFOAM employs the PIMPLE algorithm for pressure-velocity coupling, which is a combination of the SIMPLE and PISO algorithms. In the simulations, 5 PISO loops and 3 SIMPLE loops were enough to achieve converged results. An adaptive time step algorithm was used to ensure that the maximum Courant number does not exceed unity in order to keep numerical stability and accuracy.

3. RESULTS

In contrast to experimental data which presents time averaged variables, the LES model provides a transient fluctuating solution and it is necessary to calculate the time averaged variables. It was verified that the mean variables can be determined using an interval from 4 to 10 seconds because the flame reaches a pseudo-steady state in 4 seconds and converged mean variables were obtained by time integration over 6 seconds. Figure 2 exhibits the temporal convergence of mean mixture fraction and mean horizontal velocity using the mesh M4. The time-mean variables are represented using the $\langle \cdot \rangle$ operator.

Figure 3 shows the results for the horizontal mean velocity components along the flame diameter, showing the perfect agreement of $\langle U_x \rangle$ and $\langle U_y \rangle$. This implies that the mean velocity field is, as expected, axially symmetric (Xin *et al.*, 2005).

The convergence of the results for the mean temperature and axial velocity regarding the number of discretized solid angles is presented in Figure 4 for the M1 mesh. From these results using 100 and 320 discretized solid angles, it is

Table 1. Mesh Quality Statistics

Mesh	*Number of volumes*	*Maximum non-orthogonality*	*Average non-orthogonality*	*Maximum aspect ratio*
M1	465,080	38.44	4.44	22.35
M2	560,040	38.97	4.53	23.59
M3	640,030	39.20	4.52	23.69
M4	757,215	39.61	4.59	24.78

ISSN 2176-5480

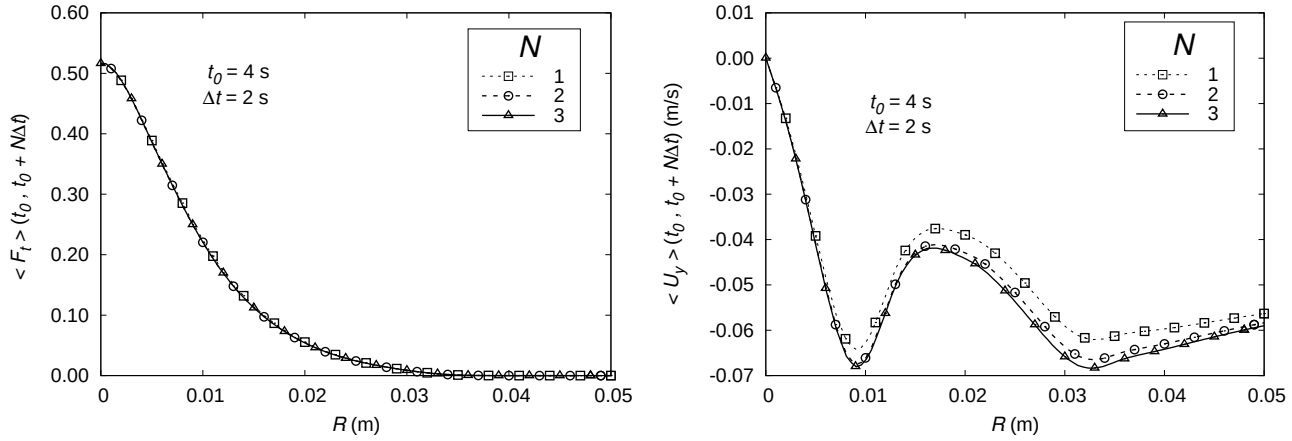

(a) (b)

Figure 2. Temporal convergence of (a) mean mixture fraction and (b) mean horizontal velocity at 5 cm above the fuel inlet.

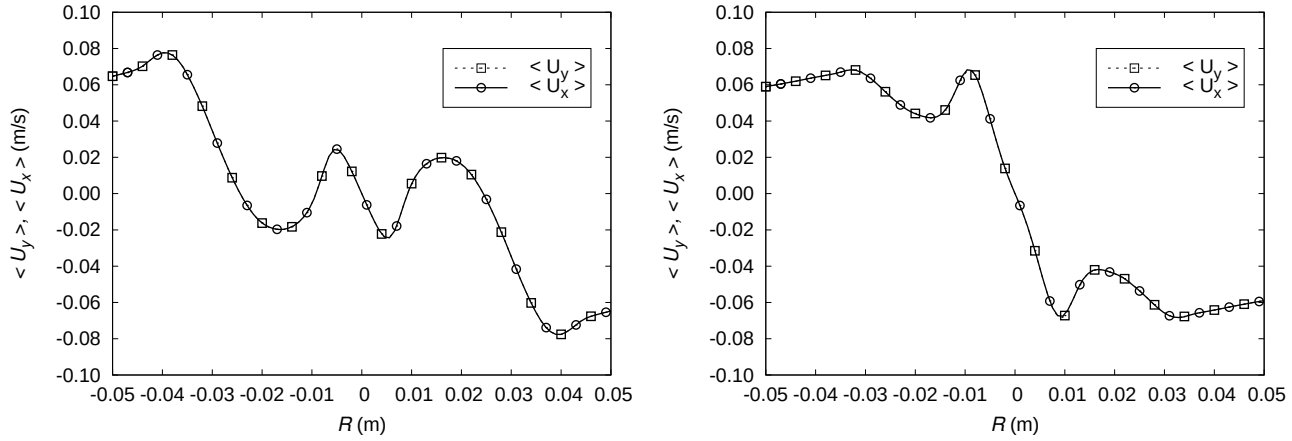

(a) (b)

Figure 3. Mean horizontal velocity components at (a) 10 and (b) 5 cm above the fuel inlet.

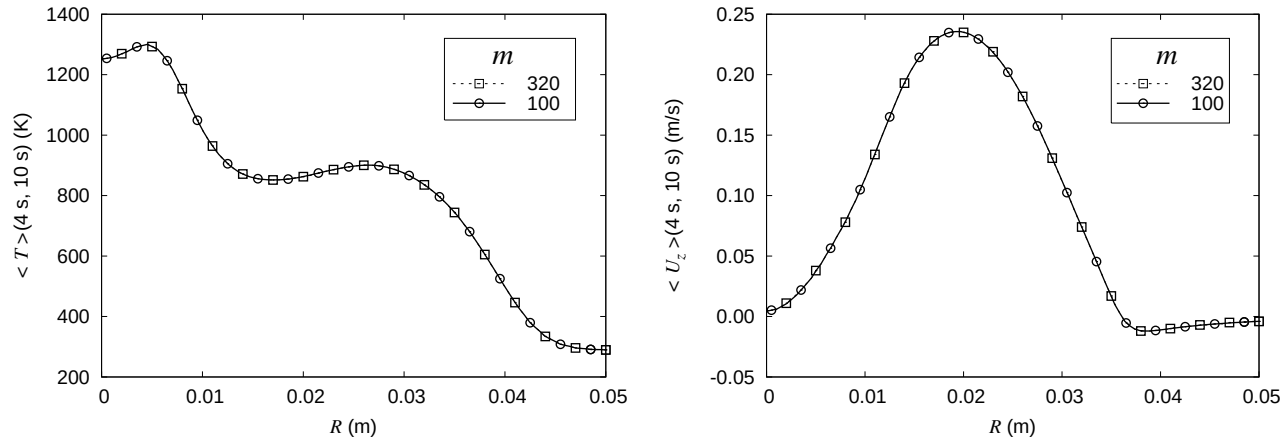

(a) (b)

Figure 4. Simulation results using 100 and 320 discretized solid angles for (a) the mean temperature at 10 cm above the fuel inlet and (b) the mean vertical velocity at 0.5 cm above the fuel inlet.

possible to verify that the number of 100 discretized solid angles is adequate, being, therefore, used in all other simulations with the other meshes.

The grid-size independence of the results was also verified and this is shown in all the following figures that compare

ISSN 2176-5480

the results of the simulations using the M3 and M4 meshes to the available experimental data.

The simulated profiles obtained for mean mixture fraction, $\langle F_t \rangle$, are shown in Fig. 5, as well as the experimental data of Xin *et al.* (2005) with 10% error bars due to the uncertainty of the measurements (Zhou and Gore, 1998).

The comparison between the results for the M3 and M4 meshes shown in Fig. 5 demonstrates a very good mesh convergence. The simulated $\langle F_t \rangle$ values are smaller than the experimental measurements at positions close to the burner but they are larger than the data for the largest distances. Therefore, the simulation gives a poorer mixing between the reagents than that expected from the data. Probably, this is due to a lower degree of the simulated turbulence, leading to a less efficient reaction and to a higher and narrower flame.

Figures 6 and 7 present the results for the horizontal, $\langle U_y \rangle$, and vertical, $\langle U_z \rangle$, components of the mean velocity, respectively. The experimental data were also plotted with 15% error bars due to the uncertainty of the velocity measurements. However, the measurement error can be as large as 25% in the low-velocity regions close to the burner inlet (Zhou and Gore, 1998).

Although the profiles of the mean horizontal velocity are well converged in Fig. 6, they do not represent well the experimental data in the outer region of the flame. This is also related to the poorer simulated mixing of the reactants, as the horizontal velocity corresponds to the air entrainment in the flame region.

Figure 7 shows that the converged results for the mean vertical velocity agree semi-quantitatively to the experimental data, which show some lack of symmetry not shown in the simulated results. Therefore, it is believed that the discrepancies between experimental and simulated data are caused by experimental uncertainty and the fact that some perturbation in the experiments broke the symmetry of the flame. Of course, some imposed perturbation in the methane inlet might be used to mimic this behavior, but this was not further explored because the asymmetry was not intense. As shown in this figure, the larger the height, the larger is the vertical velocity, which can be easily explained by the accumulated effect of the buoyant force related to the temperature increase caused by the combustion reaction. At each elevation, the mean vertical velocity profile shows a peak at a radial position which is related to the flame front location. Close to the fuel inlet, this peaks is more pronounced and, as the flame advances downstream, it gets smoother due to the turbulent mixing.

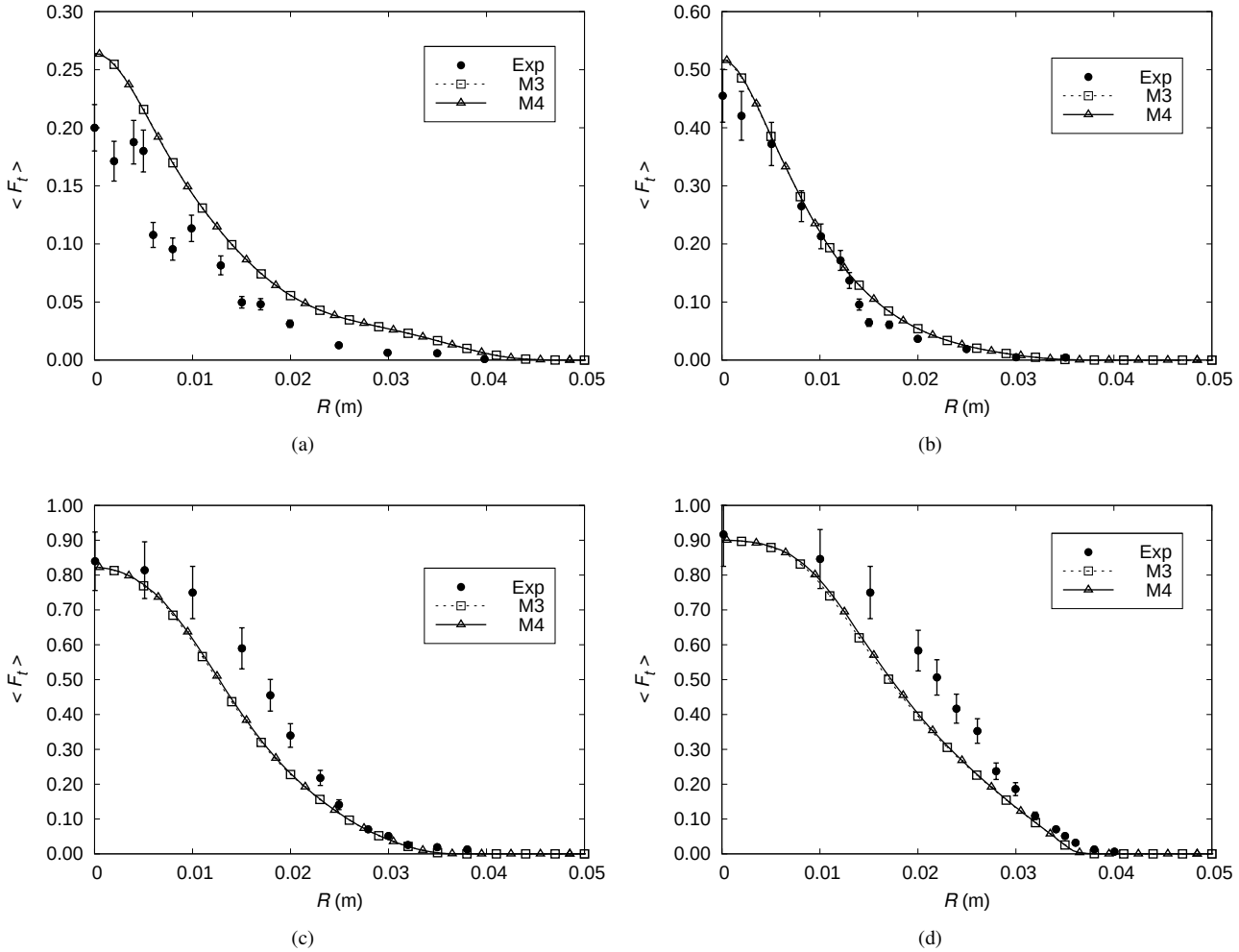

Figure 5. Mean mixture fraction profiles at (a) 10, (b) 5, (c) 1 and (d) 0.5 cm above the fuel inlet.

ISSN 2176-5480

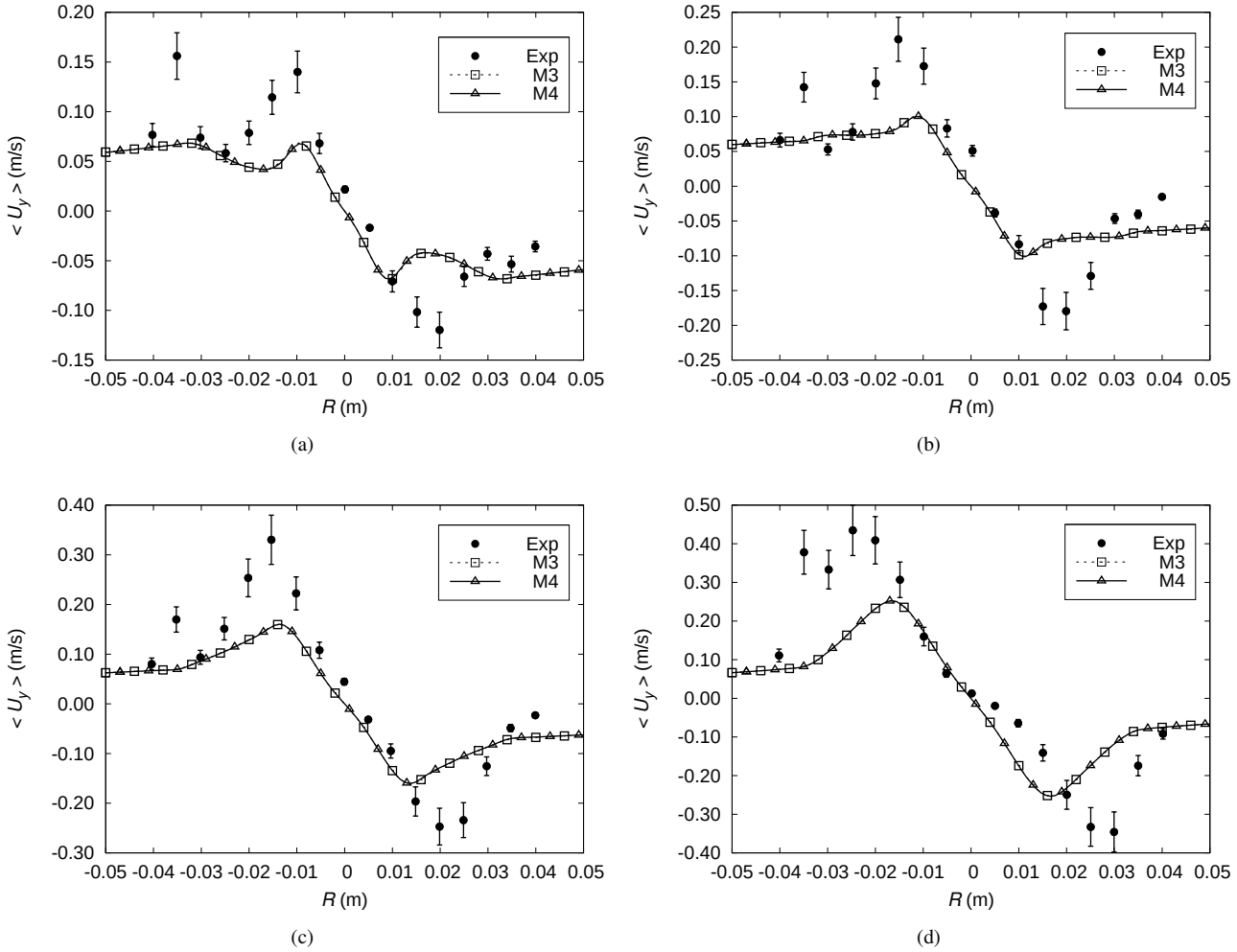

Figure 6. Mean horizontal velocity profiles at (a) 5, (b) 4, (c) 3 and (d) 2 cm above the fuel inlet.

Another important result analyzed is the Heat Release Rate (HRR). For the stoichiometric combustion with ΔH_c° = -802.310 kJ/mol and the 84.3 mg/s methane inlet flow, its value is 4.23 kW. The time average of value of HRR in the 4-10 s interval was 4.24 kW, demonstrating a very good agreement with the theoretical value.

Figure 8 shows the mean temperature radial profile at two elevation, one close to the burner and the other at a far downstream location. These temperature profiles present peak values at the reaction zones. It can be observed that the reaction zone in Fig. 8(b) is in a radial position close to 2.5 cm while it is located almost at the flame axis in Fig. 8(a). The broader temperature profile at the higher elevation is caused by the turbulent mixing of the hot product gases.

Figure 9 exhibits the vector plot of the mean vorticity projected at the $x-y$ plane located at 5 cm above the fuel inlet. In the outer region of the domain, which is outside the flame front, the vorticity vectors are oriented in the counterclockwise direction, which indicates a toroidal circulation of the air that approaches the flame from below, that is, whose radial velocity below this plane is negative. In the inner region of the flame, the vorticity vectors are oriented in the clockwise direction, which indicates another toroidal circulation of the methane that flow in the direction of the flame front from below, that is, whose radial velocity below this plane is positive. The vertical component of vorticity, not shown here, is almost zero everywhere in the domain, showing that the flame does not have a swirling motion.

Figure 10 shows the simulated instantaneous temperature profile at 6.9 s. The similarity between the flame shape depicted in this figure and the actual flame picture given by Zhou and Gore (1998) is very good. The maximum instantaneous temperature is approximately 1800 K, which is about 400 K smaller than the adiabatic flame temperature of methane, which is given by Turns (2000) as 2226 K. This was expected because the thermal radiation losses were considered in the simulation.

4. CONCLUSION

The overall agreement between the simulated and the experimental data validates the usage of FireFOAM for small size methane flames. The FVDOM thermal radiation model employed with the Planck mean absorption coefficient led

ISSN 2176-5480

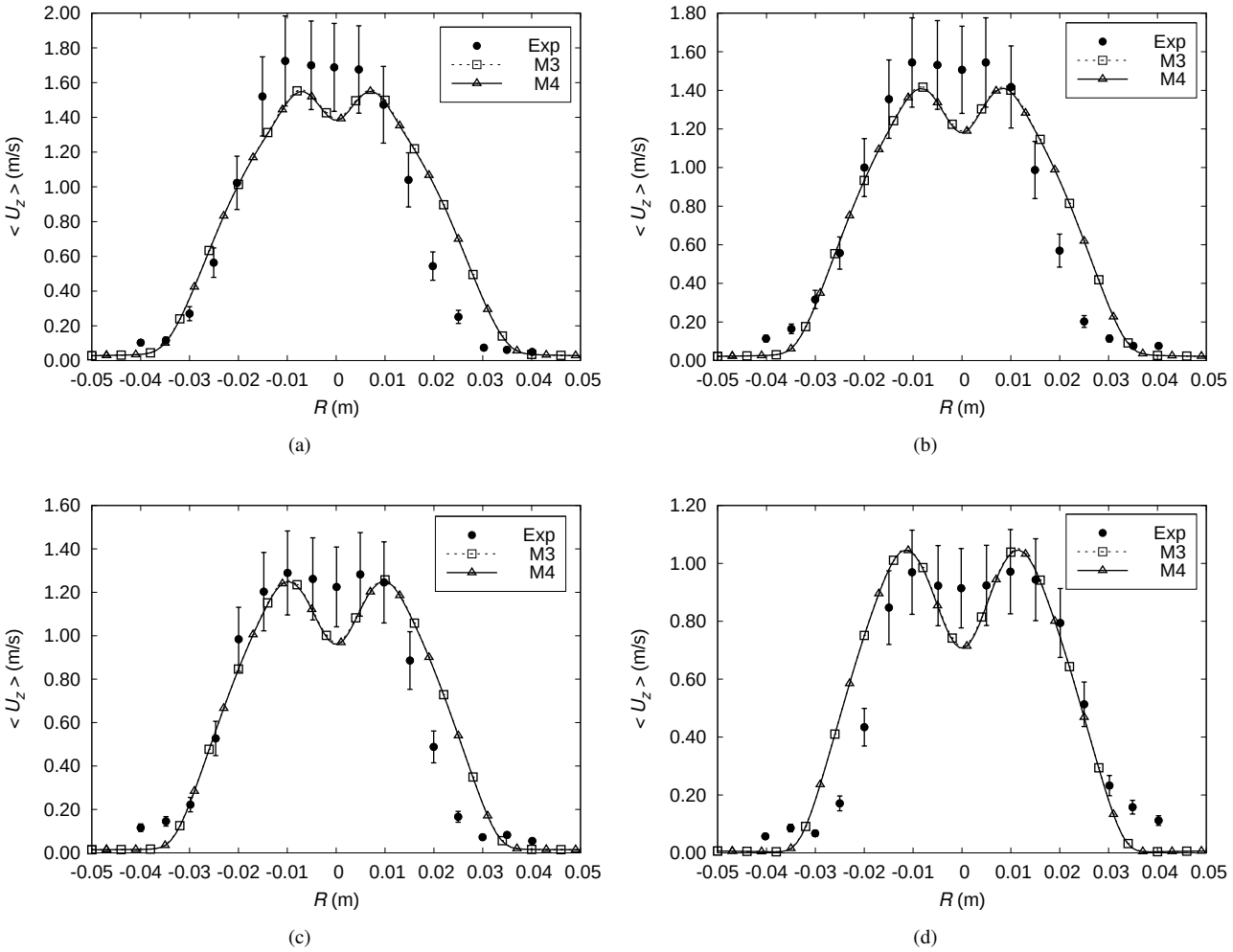

Figure 7. Mean vertical velocity profiles at (a) 6, (b) 5, (c) 4 and (d) 3 cm above the fuel inlet.

to flame temperatures in the expected range. The eddy dissipation combustion model (EDM) with single-step reaction coupled with the LES turbulence model showed to be reliable. The most important discrepancy was related to a somewhat poorer reactant mixing predicted by the model. Furthermore, some perturbations in the actual experimental conditions made the flame a little asymmetric, which could not be reproduced by simulations with an uniform fuel inlet. This certainly increased the discrepancy between the simulated and the experimental data.

For other flames, the hypotheses and simplifications employed may not be valid anymore. For heavier fuels, the

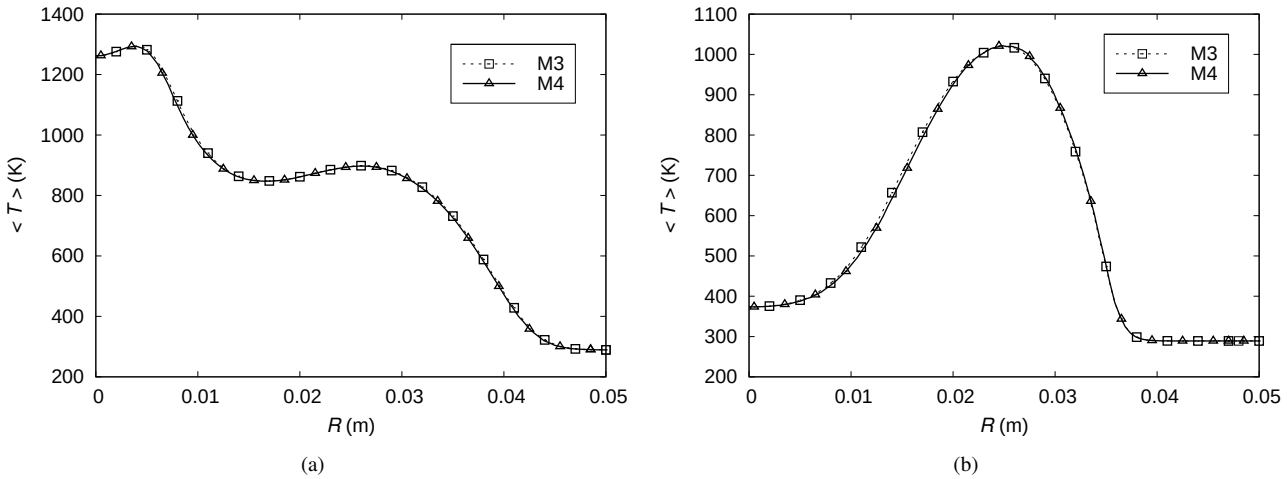

Figure 8. Mean temperature profiles at (a) 10 and (b) 0.5 above the fuel inlet.

ISSN 2176-5480

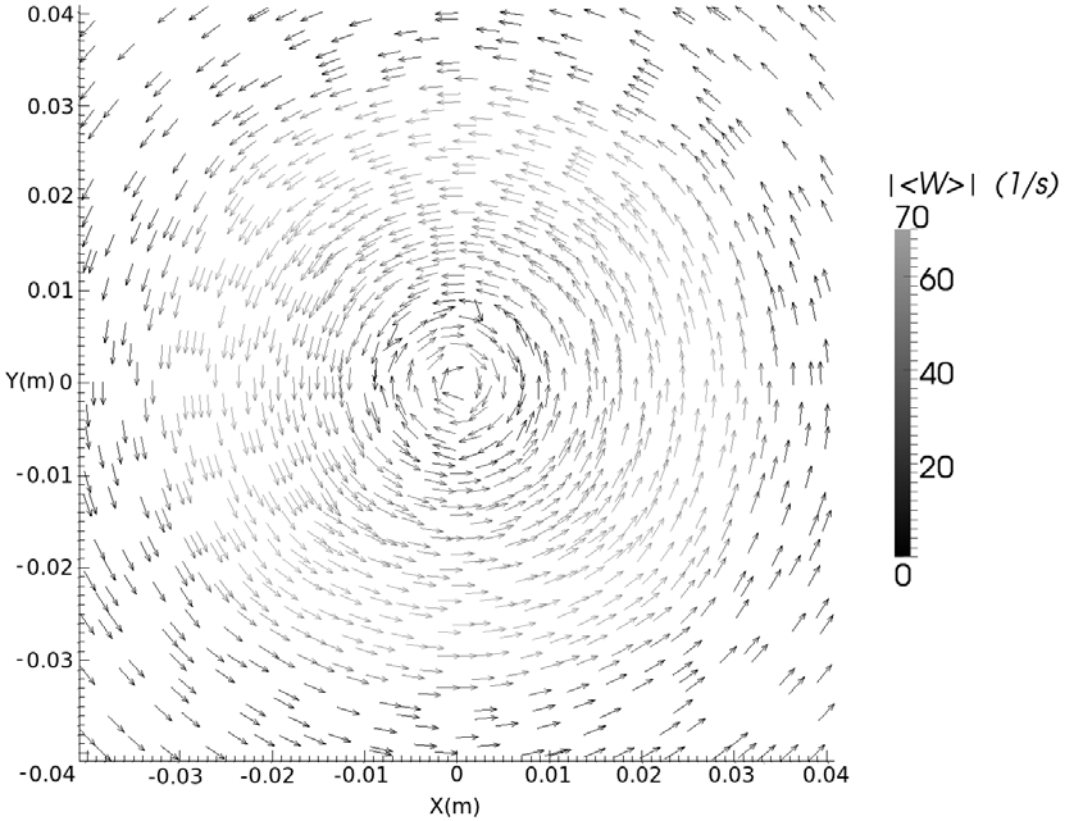

Figure 9. Mean vorticity vector plot at 5 cm from fuel inlet.

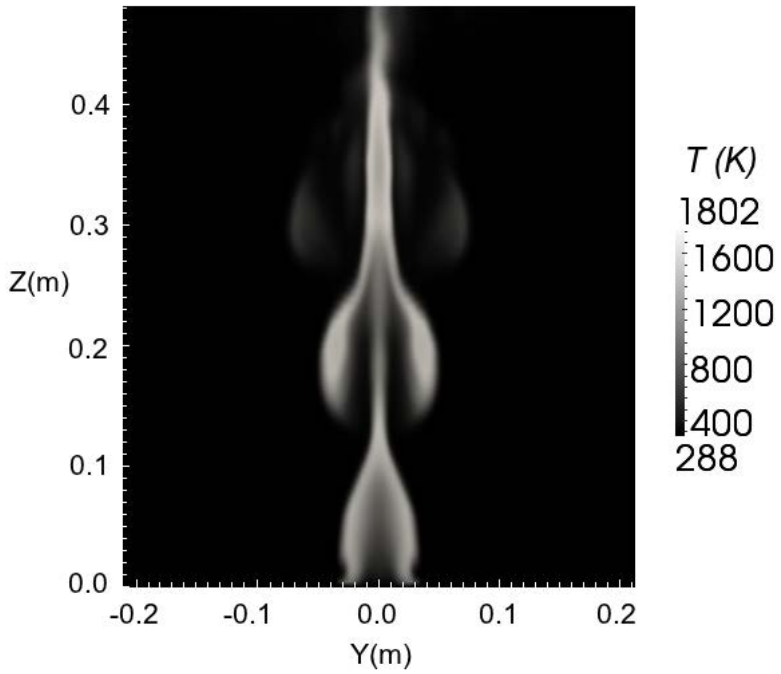

Figure 10. Instantaneous shape of the simulated temperature profile at 6.9 s.

production of soot cannot be neglected and scattering must be considered in the radiation model. For larger flames, the optical thin flame assumption is no longer valid. Besides, a many-step reaction model with intermediate species might be necessary. In order to perform complex simulations, further study is needed to implement new tools in FireFOAM to achieve reliable results.

ISSN 2176-5480

5. ACKNOWLEDGEMENTS

Paulo L. C. Lage acknowledges the financial support from CNPq, grants nos. 302963/2011-1 and 478589/2011-5, and FAPERJ, grant no. E-26/111.361/2010.

6. REFERENCES

Aspden, A.J., Day, M.S. and Bell, J.B., 2011. "Lewis number effects in distributed flames". *Proceedings of the Combustion Institute*, Vol. 33, pp. 1473–1480.

Barlow, R.S., Karpetis, A.N., Frank, J.H. and Chen, J.Y., 2001. "Scalar profiles and no formation in laminar opposed-flow partially premixed methane/air flames". *Combustion and Flame*, Vol. 127, pp. 2102–2118.

Edge, P., Gharebaghi, M., Irons, R., Porter, R., Porter, R.T.J., Pourkashanian, M., Smith, D., Stephenson, P. and Williams, A., 2011. "Combustion modelling opportunities and challenges for oxy-coal carbon capture technology". *Chemical Engineering Research and Design*, Vol. 89, pp. 1470–1493.

Erlebacher, G., Hussaini, H.Y., Speziale, C.G. and Zang, T.A., 1991. "Toward the large-eddy simulation of compressible turbulent flows". Technical report, Institute for Computer Applications in Science and Engineering.

Ferziger, J.H. and Peric, M., 2004. *Computational Methods for Fluid Dynamics*. Springer, Berlin, 3rd edition.

Lupant, D., Pesenti, B. and Lybaert, P., 2007. "Detailed characterization of flameless oxidation on a laboratory scale furnace". In *Proceedings of the European Combustion Meeting - PECM2007*. Chania, Greece.

Mangani, L., 2009. *Development and Validation of an Object Oriented CFD Solver for Heat Transfer and Combustion Modeling in Turbomachinery Applications*. Ph.D. thesis, Università degli Studi di Firenze, Firenze.

McGrattan, K., 2005. "Fire modeling: Where are we? where are we going?" In *Proceedings of the 8th International Symposium on Fire Safety Science - ISFSS2005*. Beijing, China.

Mishra, S.C. and Roy, H.K., 2007. "Solving transient conduction abd radiation heat transfer problems using the lattice boltzmann method and the finite volume method". *Journal of Computational Physics*, Vol. 223, pp. 89–107.

Modest, M.F., 2003. *Radiative Heat Transfer*. Academic Press, San Diego, 2nd edition.

Poling, B.E., Prausnitz, J.M. and O'Connell, J.P., 2001. *The Properties of Gases and Liquids*. The McGraw-Hill, Nova York, 5th edition.

Rogers, G.F.C. and Mayhew, Y.R., 1995. *Thermodynamic and Transport Properties of Fluids*. Wiley.

Siegel, R. and Howell, J.R., 1992. *Thermal Radiation Heat Transfer*. Hemisphere Publishing Corporation, Washington, 3rd edition.

Skarsbø, L.R., 2011. *An Experimental Study of Pool Fires and Validation of Different CFD Fire Models*. Master's thesis, University of Bergen, Bergen.

Smith, N., Gore, J., Kim, J. and Tang, Q., 2003. "Radiation models". 15 Feb. 2013 <http://www.sandia.gov/TNF/radiation.html>.

Turns, S.R., 2000. *An Introduction to Combustion - Concepts and Applications*. McGraw Hill, 2nd edition.

Veynante, D. and Vervisch, L., 2002. "Turbulent combustion modeling". *Progress in Energy and Combustion Science*, Vol. 28, pp. 193–266.

Wen, J.X., Kang, K., Donchev, T. and Karwatzki, J.M., 2006. "Validation of fds for the prediction of medium-scale pool fires". *Fire Safety Journal*, Vol. 42, pp. 127–138.

Xiao, H. and Jenny, P., 2011. "A consistent dual-mesh framework for hybrid les/rans modeling". *Journal of Computational Physics*, Vol. 231, pp. 1848–1865.

Xin, Y., Filatyev, S.A., Biswas, K., Gore, J.P., Rehm, R.G. and Baum, H.R., 2008. "Fire dynamics simulations of a one-meter diameter methane fire". *Combustion and Flame*, Vol. 153, pp. 499–509.

Xin, Y., Gore, J.P., McGrattan, K.B., Rehm, R.G. and Baum, H.R., 2005. "Fire dynamics simulation of a turbulent buoyant flame using a mixture-fraction-based combustion model". *Combustion and Flame*, Vol. 141, pp. 329–335.

Yeoh, G.H. and Yuen, K.K., 2009. *Computational Fluid Dynamics in Fire Engineering*. Butterworth-Heinemann, Oxford, 1st edition.

Zeng, W.R. and Chow, W.K., 2011. "A note on modeling combustion of common fuels with mixture fraction". *International Journal on Engineering Performance-Based Fire Codes*, pp. 6–11.

Zhou, X.C. and Gore, J.P., 1998. "Experimental estimation of thermal expansion and vorticity distribution in a buoyant diffusion flame". *Twenty-Seventh Symposium (International) on Combustion/The Combustion Institute*, pp. 2767–2773.

7. RESPONSIBILITY NOTICE

The authors are the only responsible for the printed material included in this paper.